Effect of temperature gradient-induced periodic deformation of CRTS III slab track on dynamic responses of the train-track system

Wang Jijun, Zhang Huanxin, Shi Cheng and Wang Meng
Railway Engineering Research Institute, China Academy of Railway Sciences Corporation Limited, Beijing, China and Railway Track Department, National Key Laboratory of High-Speed Railway Track System, Beijing, China

Received 21 June 2024
Revised 12 July 2024
Accepted 15 July 2024

Abstract

Purpose – Temperature is an important load for a ballastless track. However, little research has been conducted on the dynamic responses when a train travels on a ballastless track under the temperature gradient. The dynamic responses under different temperature gradients of the slab are theoretically investigated in this work.

Design/methodology/approach – Considering the moving train, the temperature gradient of the slab, and the gravity of the slab track, a dynamic model for a high-speed train that runs along the CRTS III slab track on subgrade is developed by a nonlinear coupled way in Abaqus.

Findings – The results are as follows: (1) The upward transmission of the periodic deformation of the slab causes periodic track irregularity. (2) Because of the geometric constraint of limiting structures, the maximum bending stresses of the slab occur near the end of the slab under positive temperature gradients, but in the middle of the slab under negative temperature gradients. (3) The periodic deformation of the slab can induce periodic changes in the interlayer stiffness and contact status, leading to a large vibration of the slab. Because of the vibration-reduction capacity of the fastener and the larger mass of the concrete base, the accelerations of both the slab and concrete base are far less than the acceleration of the rail.

Originality/value – This study reveals the influence mechanism of temperature gradient-induced periodic deformation in the dynamic responses of the train-track system, and it also provides a guide for the safe service of CRTS III slab track.

Keywords Ballastless track, CRTS III slab track, Temperature gradient, Periodic deformation, Train performance

Paper type Research paper

1. Introduction

CRTS III slab track has been extensively used in the Chinese high-speed railway due to its simple structure, high performance, low maintenance cost and high running stability (Ren, Deng, Zhang, Du, & Wu, 2021; Ye, Ren, Zhang, Zhang, & Li, 2022). Besides its advantages,

This work has been supported by National Key R&D Program of China [Grant No. 2022YFB2603400], R&D Project of China State Railway Group Corporation Limited [Grant No. P2021G053] and R&D Project of China Academy of Railway Science Corporation Limited [Grant No. 2023YJ200]. The contents of this paper only reflect the authors' views; the Joint Undertaking is not responsible for any use that may be made of the information contained in the paper.

Railway Sciences
Vol. 3 No. 4, 2024
pp. 437-452
Emerald Publishing Limited
e-ISSN: 2755-0915
p-ISSN: 2755-0907
DOI 10.1108/RS-06-2024-0020

CRTS III slab track has its limitations. One limitation is that segmented track slabs are sensitive to the temperature load. The initial deformation and gap are usually caused by the temperature gradient of the ballastless track, and they exhibit upward or downward warping deformation with a period of the length of one track slab.

Considerable experimental and theoretical efforts have been directed toward revealing the temperature distribution and the mechanical performance of the ballastless track. Liu *et al.* studied the temperature distribution and its influence factors in the asphalt supporting layer of CRTS III slab track by combining numerical simulation and *in situ* measurement (Liu, Chen, Yang, Cai, & Yang, 2020). Yu *et al.* found that the daily extreme values of monthly axial uniform temperature and the daily maximum temperature gradient obey certain statistical laws and the large tensile stress appears at the corner or middle of the slab (Yu, Xie, & Tian, 2019). Liu *et al.* simulated chloride transport within the track structure by boundary condition models based on high-precision climate data and revealed the temperature acceleration effect of solar radiation heating on chloride diffusion (Liu, Song, Liu, Zhang, & Yu, 2023). Zhong *et al.* measured the daily changing temperature on a testing platform constructed in the open field and analyzed the interface stress and curling behavior of slab tracks based on a three-dimensional (3D) finite element model (FEM) (Zhong, Gao, & Zhang, 2018). Li *et al.* investigated the interface damage of CRTS II slab track under temperature load with a 3D FEM using the cohesive element (Li, Chen, Wang, Shi, & Chen, 2020).

The train load is another crucial load for railway tracks. Many researchers have focused on the mechanical characteristics and damage of the ballastless track caused by both the train and temperature loads. Xu *et al.* studied the stresses in CRTS I slab track under combined loads using 3D FEM (Xu & Li, 2012). Zhang *et al.* analyzed the filling layer de-bonding of CRTS II slab track based on viscoelastic theory under temperature and train loads (Zhang, Wu, Gao, Yan, & Cai, 2019). Song *et al.* used the track irregularities caused by the temperature load as an excitation and conducted the coupled dynamic analysis for CRTS II slab track (Song, Zhao, & Zhu, 2014). Xu *et al.* developed a dynamic train-track coupling model to investigate the system dynamic responses under the temperature gradient of CRTS III slab track with different amplitudes (Xu *et al.*, 2022).

To date, many studies have contributed to the temperature distribution, mechanical behaviors and damage of ballastless track caused by the temperature load or by the combined train and temperature loads (Ren, Li, Yang, Wang, & Xie, 2016; Song *et al.*, 2014; Xu & Li, 2012; Zhu *et al.*, 2018). However, most of these studies focused on static analysis, whereas the system dynamics under the joint action of temperature and train load remain elusive (Xu *et al.*, 2022; Zhu & Cai, 2014). Additionally, the recent train–track coupling dynamic analysis does not consider the nonuniform vertical stiffness under the slab caused by the gaps between the interlayers of the ballastless track and the 3D multi-layer structure of the slab track (Song *et al.*, 2014; Xu *et al.*, 2022; Zhu & Cai, 2014).

In this work, we establish a high-speed 3D train-ballastless track on the subgrade coupling dynamic model under the train load, the gravity load and the temperature gradient of the track system. The temperature gradient-induced deformation of CRTS III slab track and its effect on stresses, vertical stiffness under the slab and dynamic responses of the track system and the train performance are analyzed and discussed in depth. This work reveals the influence of temperature gradients on the dynamic responses of train-track system, which can provide the reference for the design of ballastless track structures and maintenance during operation.

2. 3D train-ballastless track on subgrade coupling dynamic model

In this model, the structure layers are consistent with the actual track structures. Therefore, the calculation results can present the spatial distributions of the dynamic and static

response of the track structure and ensure that the train performance calculated by the 3D train-track coupling dynamic model is more precise than those calculated by the 2D model. To reduce the calculation cost, the structures that provide elastic cushioning, such as fasteners and cushions, are often simplified to spring dampers in the dynamic calculation, which is also adopted in our model. For the train, because this work only focuses on wheel-rail forces and car body vibration, the train sub-model is modeled as a multi-rigid body system. The wheel-rail interaction is described by the Hertzian nonlinear contact theory (Lei & Noda, 2002; Zhai & Cai, 1997). Figure 1 shows the schematic of the coupling dynamic model established by the commercial software *Abaqus*. In the model, a high-speed train moves forward along the CRTS III slab track with periodic temperature deformation on subgrade at a constant speed.

2.1 High-speed train sub-model

A typical train consists of the car body, bogie, wheel and primary and secondary suspensions. The car body, bogie and wheel are treated as rigid bodies, each with 6 degrees of freedom. The primary and secondary suspensions are used to connect the bogie and wheel, and the car

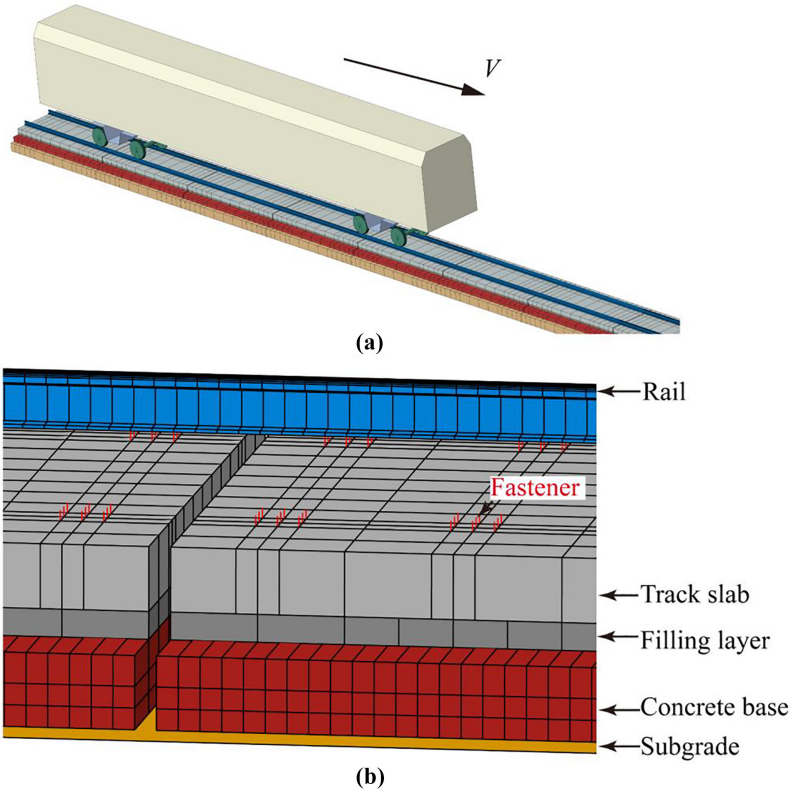

Note(s): (a) Train track dynamic model; (b) finite element model of CRTS III slab track

Source(s): Authors' own work

Figure 1.
The schematic of the 3D train-track on subgrade coupling dynamic model

body and bogie, respectively. Due to the complex and nonlinear characteristics of the suspension systems, the suspensions are simplified by the three directional linear spring-damper elements. Taking CRH380-B high-speed train parameters as an example, the parameters are given in Table 1.

2.2 CRTS III slab track on subgrade sub-model

The CRTS III slab track consists of seven parts, including the rail, fastener, track slab, filling layer, concrete base, isolation layer and elastic cushion. The rail, track slab, filling layer and concrete base are modeled by 3D linear elastic solid elements. The fastener is reduced to a spring-damper element. The isolation layer, elastic cushion and the elastic support of the subgrade are modeled as the contact elements with the surface stiffness, which reflects the dynamic interlayer contact relation. All parameters used in the track sub-model are listed in Table 2, in which the static/dynamic stiffnesses of the fastener are listed (TB 10015-2012, 2013). The total model length is 136.01 m, and the enlarged views of this model are shown in Figure 1. In the model, 24 slabs with a length of 5.6 m and 12 concrete bases with a length of 11.27 m are modeled, respectively. The rail is supported discretely by fasteners at a spacing of 0.63 m. The wheel-rail contact is described by Hert contact and Kalker creep theory. The starting and braking conditions are not considered in the calculation, so the longitudinal dynamic characteristics of the model are negligible.

2.3 Numerical simulation

The dynamic responses of the train-track system are closely related to the initial temperature deformation. Therefore, a static analysis is firstly performed under the gravity of the train-track system and different temperature gradients of the slab track, i.e. −45, −22,5, 0, 22.5, 45, 67.5, 90 °C/m. We obtain the mechanical fields, interlayer contact state and stiffness at the initial state. By applying a small uniform pressure on the slab track, the increments in vertical displacement Δu and nodal force ΔF_n of the slab can be obtained. Subsequently, the vertical stiffness under the rail can be calculated by using the stiffness formula: $k_{ur} = \Delta F_n / \Delta u$. Similarly, the variations in void height $\Delta\delta$ and contact force ΔF_c under the slab can be obtained, allowing for the calculation of the vertical stiffness under the slab by using the stiffness formula: $k_{us} = \Delta F_c / \Delta\delta$.

Component	Mass (kg)	Rolling inertia (kg·m^2)	Nodding inertia (kg·m^2)	Shaking head inertia (kg·m^2)
Car body	48,000	1.15×10^5	2.7×10^6	2.7×10^6
Bogie	3,200	3,200	7,200	6,800
Wheel	2,400	1,200	/	1,200

Component	Longitudinal stiffness (kN/m)	Lateral stiffness (kN/m)	Vertical stiffness (kN/m)	Longitudinal damp (kN·s/m)	Lateral damp (kN·s/m)	Vertical damp (kN·s/m)
Primary suspension system	9.0×10^3	3.0×10^3	1.04×10^3	0.0	0.0	5
Secondary suspension systems	0.24×10^3	0.24×10^3	0.40×10^3	10	30.0	6

Table 1.
Parameters for train submodel

Source(s): Parameters courtesy of Zhao (2015)

Component	Size (m×m×m)	Material	Young's modulus (MPa)	Poisson ratio	Density (kg/m^3)	Thermal coefficient (℃$^{-1}$)
Rail		Steel	2.1×10^5	0.3	7,800	
Track slab	$5.6 \times 2.5 \times 0.21$	Concrete	3.6×10^4	0.2	2,500	10^{-5}
Filling layer	$5.6 \times 2.5 \times 0.09$	SCC	3.4×10^4	0.167	2,500	
Concrete base	3.1×0.30	Concrete	3.4×10^4	0.2	2,500	
Component	Longitudinal static/dynamic stiffness (kN/mm)	Lateral static/dynamic stiffness (kN/mm)	Vertical static/dynamic stiffness (kN/mm)	Longitudinal damp (kN·s/m)	Lateral damp (kN·s/m)	Vertical damp (kN·s/m)
Fastener	12/30	50/75	35/50	75	60	60
Component				Surface stiffness (MPa/m)		
Isolation layer				400		
Elastic cushion				120		
Subgrade				76		

Source(s): Parameters courtesy of Zhao (2015) and Zhao *et al.* (2024)

Table 2.
Parameters for CRTS III slab track on subgrade submodel

Taking the static analysis results as the initial conditions, the train moves forward 120 m at 200–400 km/h. The time step of dynamic simulations is 5×10^{-6} s to account for the high-frequency dynamic responses and numerical stability. We obtain the dynamic responses of the coupled system and the train performance based on two typical initial states under the temperature gradient of −45 and 90 ℃/m (TB 10082-2017, 2017). To discuss the effect of temperature deformation on dynamic responses, The periodic irregularity caused by temperature warping deformation is superimposed on the initial random irregularity spectrum of the high-speed railway (TB/T 3352-2014, 2014). The nodes and elements in the middle of two adjacent fasteners and at the fastener positions from the 9th and 14th slab are chosen as the output range. The validity of the model has been verified in our previous work (Zhao *et al.*, 2024). Under the experimentally measured temperature gradient, the simulated vertical displacements at the middle and end of the slab are in good agreement with the experimental measurements at the same positions. The measured results are slightly larger than the simulated ones, with the peak deviation being less than 10%, as shown in Figure 2.

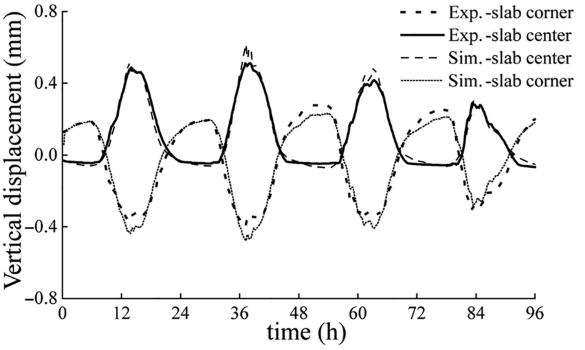

Source(s): Figure courtesy of Zhao *et al.* (2024)

Figure 2.
Comparison between experimentally measured and simulated vertical displacements of the slab

3. Effects of temperature gradients on the initial state of CRTS III slab track

3.1 Periodic deformation and mechanical behaviors of slab track under temperature gradient

At the initial state of CRTS III slab track, the mechanical responses of the track system are generated by the temperature load. Temperature gradient along the thickness of the track slab induces the initial bending moment, which is shown in Figure 3(a). The magnitudes of both positive and negative moments are proportional to the temperature gradient, and the maximum initial moments appear in the middle of the slab, decreasing toward both ends of the slab. Therefore, the vertical displacement distribution under the rail of the slab in Figure 3(b) also has the same relation with the temperature gradient of the slab. Additionally, the maximum positive and negative displacements occur in the middle and at the end of the slab under a positive temperature gradient, respectively. Contrarily, they occur at the end and in the middle of the slab under a negative temperature gradient, respectively.

The upward transmission of the deformations of the slab causes the change in initial fastener forces, as shown in Figure 4(a). The maximum initial fastener forces appear at or near the slab end. The maximum fastener tension force when $\Delta T = 45\,^{\circ}\mathrm{C/m}$ is 1.62 kN, which is larger than that of 0.82 kN when $\Delta T = -45\,^{\circ}\mathrm{C/m}$. When $\Delta T = 90\,^{\circ}\mathrm{C/m}$, the maximum fastener tension force is 5 kN, reaching about 28% of the allowable tension force of 18 kN for the WJ-8 fastener system, and should be considered in practical engineering (TB 10082-2017, 2017). The fastener forces acting on the rail cause the bending moment of the rail. As shown in Figure 4(b), because the fastener forces occur in the transition between positive and negative values at the first and second fasteners, the bending moment of the rail changes identically in this range. The stress of rail calculated with the maximum bending moment of rail 4.02 kN·m is about 13.11 MPa, which is far less than the allowable rail stress of 350 MPa (TB 10015-2012, 2013). The fluctuation of fastener forces induces vertical displacements, and the bending moment of the rail causes rotation angles of the rail. Therefore, the maximum displacements of rail occur in the middle or at the end of the slab, whereas the maximum rotation angles of rail occur near the end of the slab, as shown in Figure 4(c–d). The initial deformations of rail when $\Delta T = 45\,^{\circ}\mathrm{C/m}$ are smaller than those when $\Delta T = -45\,^{\circ}\mathrm{C/m}$. When $\Delta T = 90\,^{\circ}\mathrm{C/m}$, the maximum displacement of rail is 0.72 mm, which is about six times larger than that when $\Delta T = -45\,^{\circ}\mathrm{C/m}$. Thus, the periodic irregularity of rail when $\Delta T = 90\,^{\circ}\mathrm{C/m}$ more probably affects the train performance.

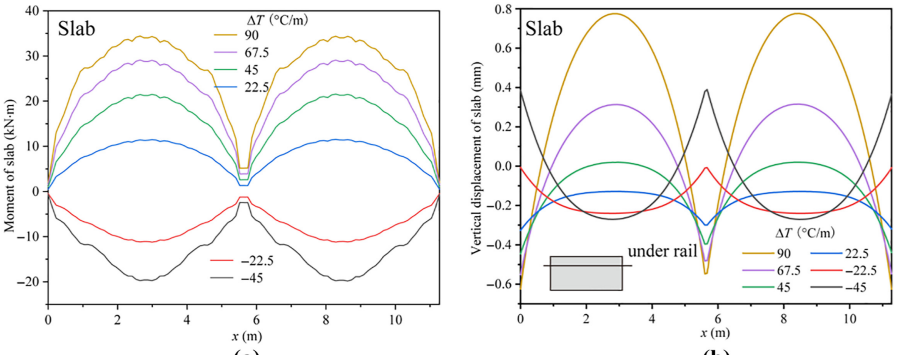

Figure 3.
Initial periodic deformation and its mechanical origin of the slab under different temperature gradients

Note(s): (a) Moment of slab; (b) vertical displacement of slab

Source(s): Authors' own work

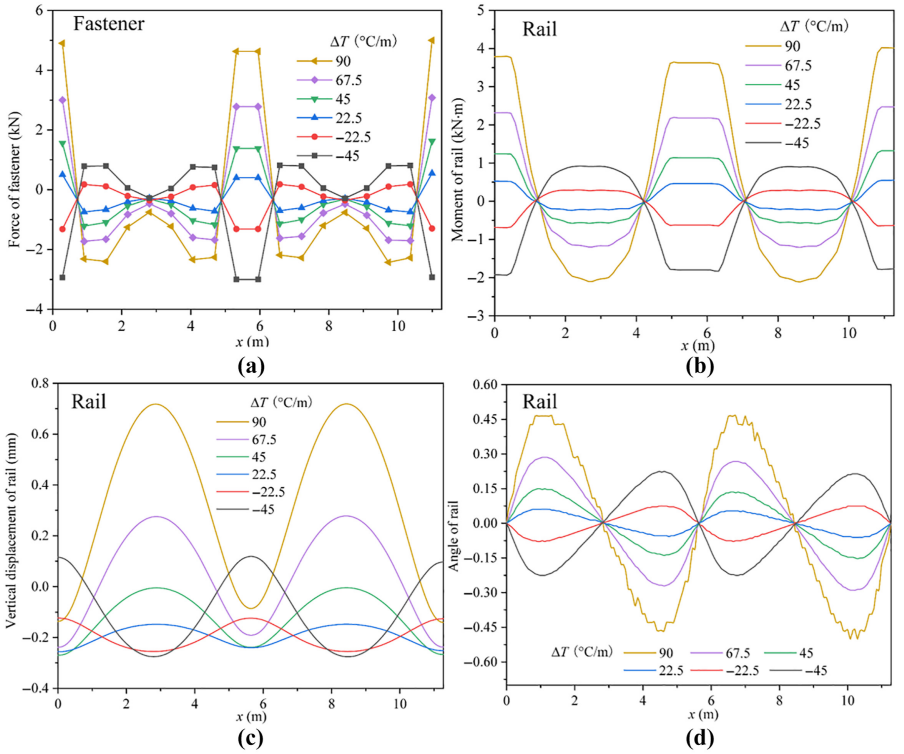

Note(s): (a) Force of fastener; (b) moment of rail; (c) vertical displacement of rail; (d) angle of rail

Source(s): Authors' own work

Figure 4. Initial periodic deformation and its mechanical origin of rail under different temperature gradients

As shown in Figure 5(a) and (b), due to the geometric constraint of limiting structures, the maximum principal stress of the slab occurs near the end of the slab under a positive temperature gradient. However, that occurs in the middle of the slab under a negative temperature gradient. The maximum principal stress when $\Delta T = -45\,^{\circ}\mathrm{C/m}$ is higher than that when $\Delta T = 90\,^{\circ}\mathrm{C/m}$, whereas the average stress when $\Delta T = 90\,^{\circ}\mathrm{C/m}$ is higher than that when $\Delta T = -45\,^{\circ}\mathrm{C/m}$. The maximum principal stress is 1.37 MPa, which is about 48% of the allowable concrete tension stress of 2.85 MPa of C60 grade concrete in the design code (GB 50010-2010, 2010). Therefore, the slab stress is critical for the slab track design and should be considered.

As shown in Figure 5(c) and 5(d), the maximum principal stress of the concrete base occurs at the slab corner in the middle of the concrete base under a positive temperature gradient. However, that occurs in the middle of the slab under a negative temperature gradient. The magnitude of the maximum principal stresses of the concrete base when $\Delta T = -45\,^{\circ}\mathrm{C/m}$ and $\Delta T = 90\,^{\circ}\mathrm{C/m}$ are 0.41 MPa and 0.60 MPa as observed in Figure 5(c) and 5(d), respectively. The stresses of the concrete base are much less than those of the slab.

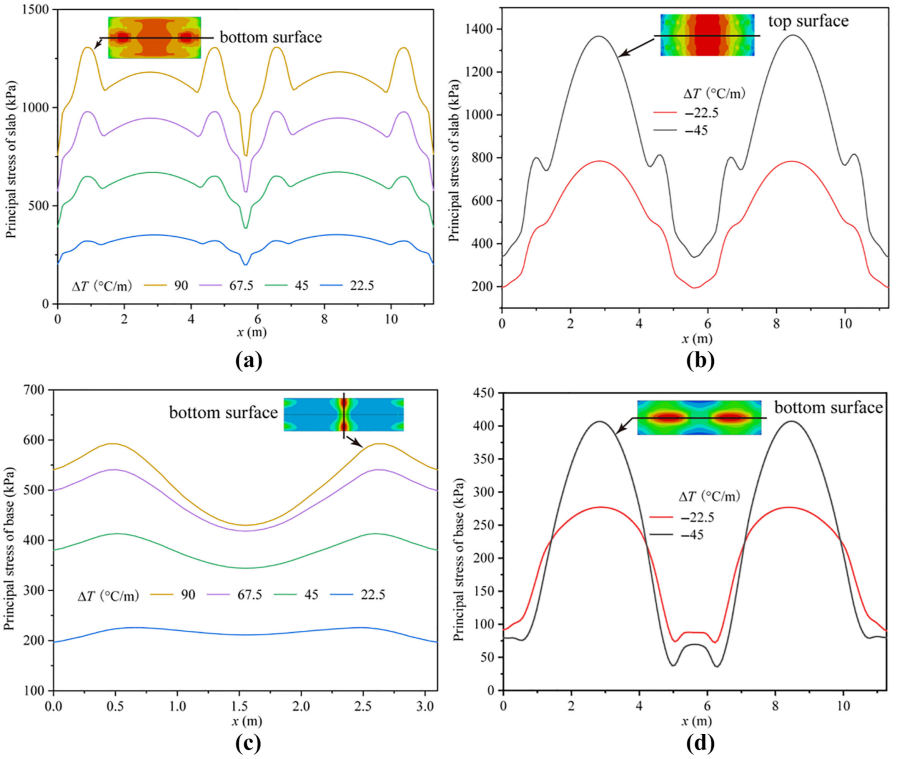

Figure 5.
Initial stresses of the slab and concrete base under different temperature gradients

Note(s): (a) Principal stress of slab for positive temperature gradients; (b) principal stress of slab for negative temperature gradients; (c) principal stress of base for positive temperature gradients; (d) principal stress of base for negative temperature gradients

Source(s): Authors' own work

3.2 Interlayer interaction of slab track under temperature gradient

Figure 6 shows the initial contact stresses under the slab when $\Delta T = -45\,℃/m$ and $\Delta T = 45\,℃/m$. One can find that the initial contact stresses are not uniformly distributed and concentrate in the middle when $\Delta T = -45\,℃/m$ and at the corner of the slab when $\Delta T = 45\,℃/m$ with a maximum value, respectively. Moreover, the side of the limiting structure in contact with the base presents the contact stresses with a large value. The magnitude of the maximum contact stresses of the slab when $\Delta T = -45\,℃/m$ and $\Delta T = 45\,℃/m$ are 0.04 MPa and 0.12 MPa as observed in Figure 6(a–b), respectively. It can be also deduced from contact statuses in Figure 7(a) and 8(a) that there are initial gaps at the end of the slab when $\Delta T = -45\,℃/m$ and in the middle of the slab when $\Delta T = 90\,℃/m$.

When $\Delta T = 0\,℃/m$, the stiffnesses under the slab and rail are uniformly distributed. With the change of interlayer contact status, the stiffnesses transit into periodic distribution like the deformation of the slab. Under a positive temperature gradient, the stiffness profiles are smaller in the middle of the slab and larger at both ends. As ΔT increases, the overall stiffness decreases significantly, in the middle of the slab, the stiffness under the rail

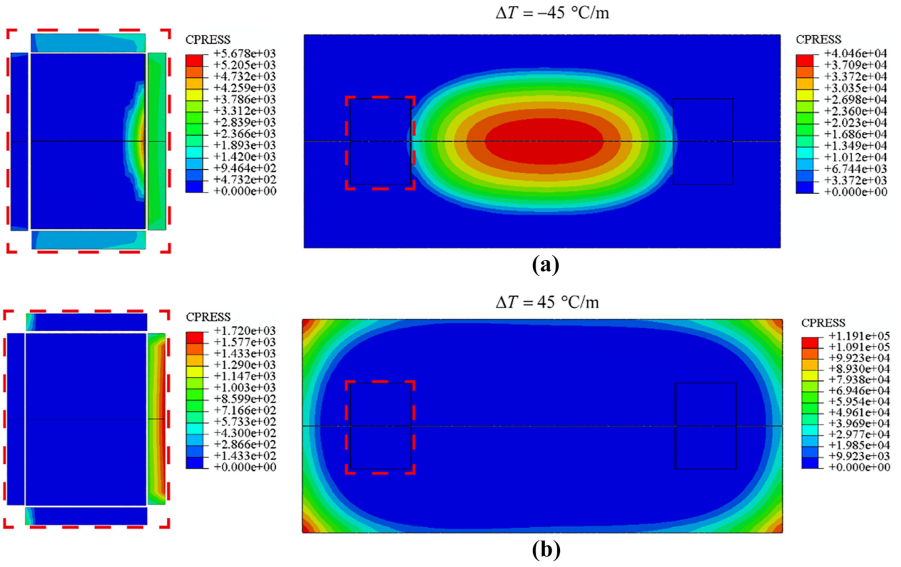

Note(s): (a) Contact stress of the slab when $\Delta T = -45$ °C/m; (b) contact stress of the slab when $\Delta T = 45$ °C/m

Source(s): Authors' own work

Figure 6.
Initial contact stresses of slab for negative and positive temperature gradient

decreases to 34.20 kN/m when $\Delta T = 90\,^{\circ}\mathrm{C/m}$ and the stiffness under the slab decreases to zero [Figure 7(b–c)]. Under a negative temperature gradient, the stiffness profiles are smaller at the end of the slab and larger in the middle. As ΔT increases, at both ends of the slab, the stiffness under the rail decreases to 84.13 kN/m when $\Delta T = -45\,^{\circ}\mathrm{C/m}$ and the stiffness under the slab decreases to zero [Figure 8(b–c)]. As shown in Figure 7(c) and Figure 8(c), when the void height is close to zero, the stiffness under the slab approaches that of the standard state of the slab track when $\Delta T = 0\,^{\circ}\mathrm{C/m}$. As the void height increases, the stiffness rapidly decreases to zero. Therefore, the temperature gradient affects the energy transmission by changing the stiffness under the slab and contact status.

The influences of the temperature gradient of the slab on the maximum contact pressure and void height are shown in Figure 9. With the increasing temperature gradient of the slab, the maximum values for these items increase. The maximum pressure under slab in Figure 9(a) when $\Delta T = 90\,^{\circ}\mathrm{C/m}$ is 237.5 kPa, and the value is much larger than that when $\Delta T = -45\,^{\circ}\mathrm{C/m}$. The maximum initial gap height in Figure 9(b) when $\Delta T = 90\,^{\circ}\mathrm{C/m}$ is about 1.21 mm. The initial gaps will affect the dynamics response of the track system because of the open-closure clapping action of the slab when a train move passes through the region with initial gaps.

4. Effect of temperature gradient-induced deformation on dynamic responses for the coupled systems

The effects of the temperature gradient of slab track on the maximum dynamic responses for different parameters for typical temperature loads, i.e. $\Delta T = -45, 0, 90\,^{\circ}\mathrm{C/m}$, and train velocities, i.e. 200 km/h–400 km/h are shown in Figures 10 and 11, and its sampling time

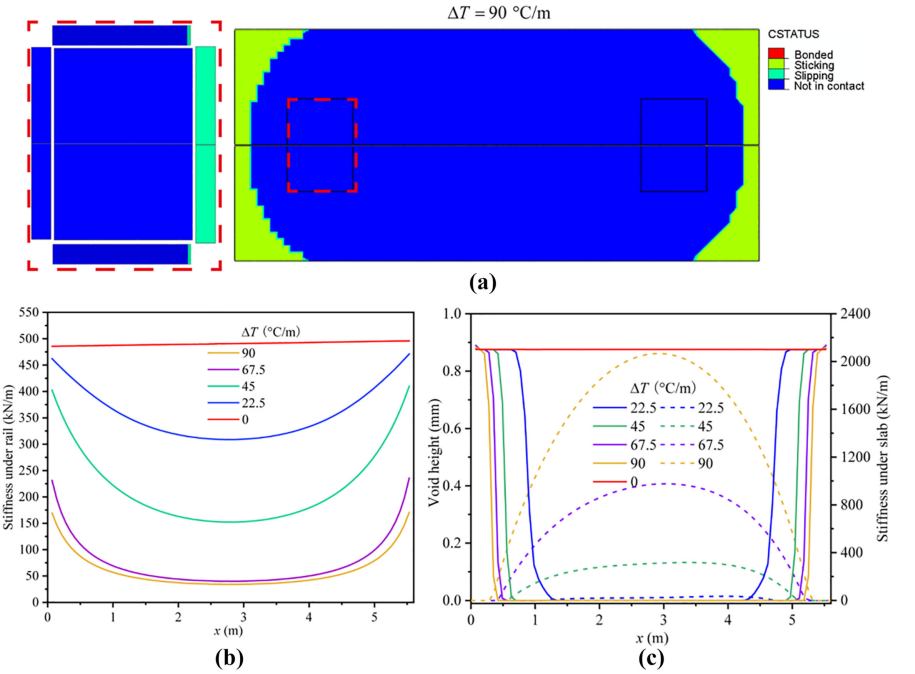

Figure 7.
Initial stiffnesses under the rail and the slab for positive temperature gradients

Note(s): (a) Contact status under slab when $\Delta T = 90$ °C/m; (b) stiffness under rail for positive temperature gradients; (c) stiffness under slab (solid line) and void height (dotted line) for positive temperature gradients

Source(s): Authors' own work

interval is 0.0005s. The maximum dynamic responses increase significantly with the rise in train velocities. However, compared with the constant temperature, the maximum dynamic responses under the temperature gradient only increase slightly.

As shown in Figure 10(a), the maximum car body acceleration of 0.05 m/s^2 due to the temperature gradient of the slab track is only 3.8% of the allowable car body acceleration of 0.13g (TB 10621-2014, 2014) and can be neglected in practical engineering. Additionally, as shown in Figure 10(b-d), the maximum accelerations of rail, slab and concrete base under a temperature gradient of 90 °C/m is larger than that under a temperature gradient of −45 °C/m due to the effect of the gap under the slab [Figure 10(b)]. Because the fastener has the vibration-reduction capacity and can reduce the vibration induced by the gap under the slab, the acceleration of the slab is less than the acceleration of the rail [Figure 10(c)]. The acceleration of the slab is more than that of the concrete base because the mass of the concrete base is larger than that of the slab [Figure 10(d)]. The large vibration of the slab track is harmful to the surrounding environment and is recommended to be considered in practical engineering.

In terms of running safety evaluation, the maximum wheel-rail vertical force, the rate of wheel load reduction and the derailment coefficient increase with the train velocity, and the increase rate is also proportional to the velocity (Figure 11). Comparing the maximum wheel-rail force when v = 200 km/h with that when v = 400 km/h, the wheel-rail force

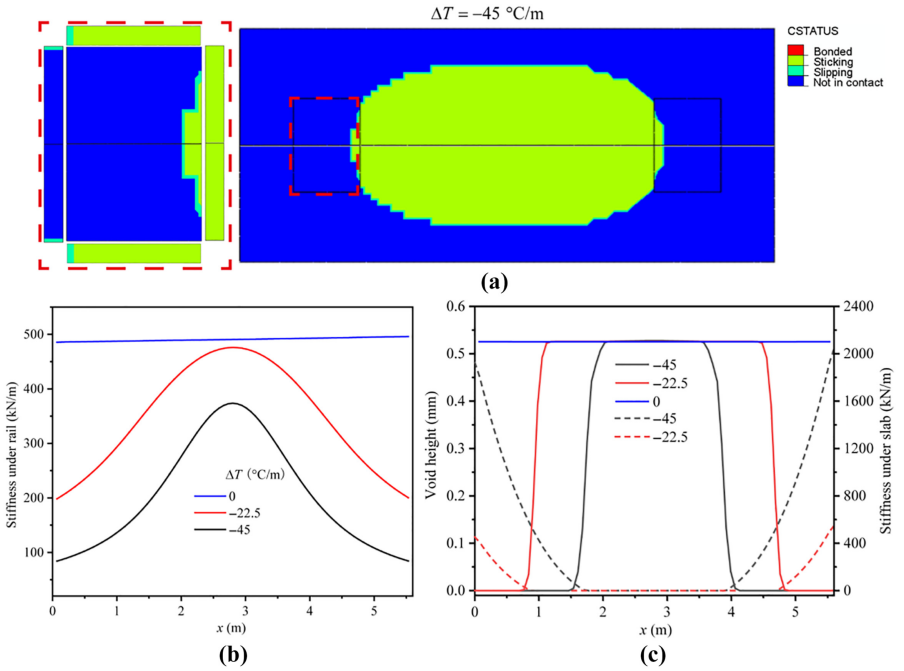

Note(s): (a) Contact status under slab when $\Delta T = -45$ °C/m; (b) stiffness under rail for negative temperature gradients; (c) stiffness under slab (solid line) and void height (dotted line) for negative temperature gradients

Source(s): Authors' own work

Figure 8.
Initial stiffnesses under the rail and under the slab for negative temperature gradients

increases by 2.4 times [Figure 11(a)]. The maximum wheel-rail force is 141.22 kN is quite close to the allowable wheel-rail force of 170 kN (TB 10621-2014, 2014), so it is necessary to pay attention to the wheel-rail force when the train velocity reaches 400 km/h. Additionally, the maximum rate of wheel load reduction and the derailment coefficient are 0.43 and 0.44, respectively, which do not reach the limit value, as shown in Figure 11(b–c). Therefore, the running safety satisfies the requirements of each response index (TB 10621-2014, 2014).

5. Conclusions

In this work, considering the temperature gradient and the train load, we established a 3D high-speed train-track on the subgrade coupling dynamic model and studied the effect of temperature gradient-induced periodic deformation on static and dynamic responses of the track system and train performance. The following conclusions can be drawn.

(1) The temperature gradient causes the bending of the slab track. Due to the constraint of fasteners, the bending load is transferred upward to the rail, leading to the periodic irregularity of the track. The maximum positive and negative

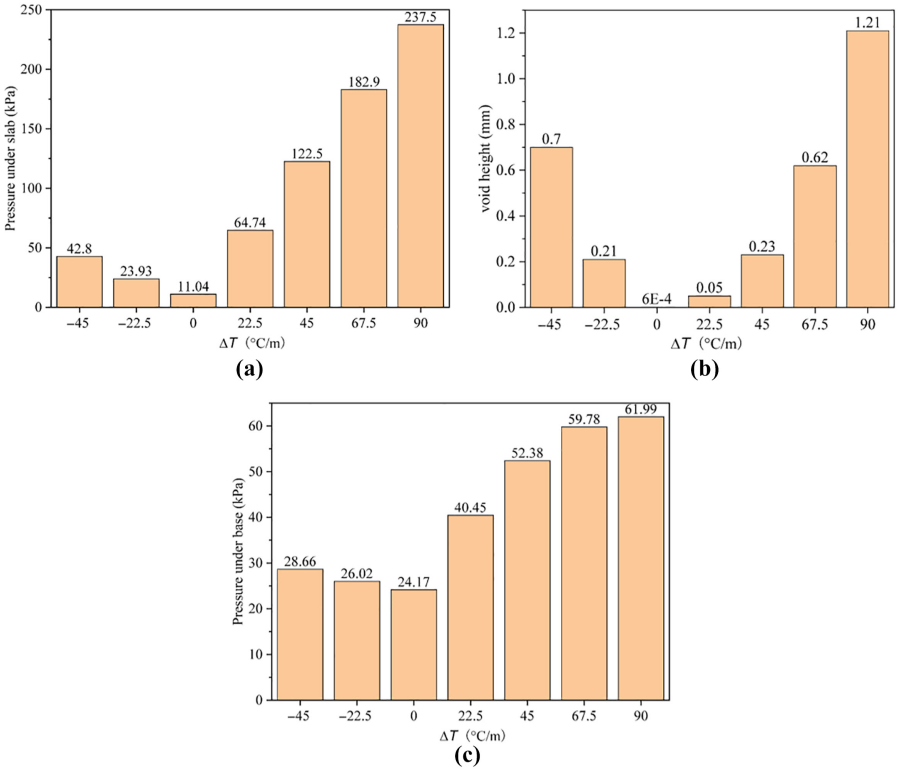

Figure 9.
Relations between the temperature gradient of the slab and maximum initial contact behaviors

Note(s): (a) Pressure under slab; (b) void height; (c) pressure under base

Source(s): Authors' own work

displacements occur in the middle and at the end of the slab under a positive temperature gradient, respectively. Conversely, they occur at the end and in the middle of the slab under a negative temperature gradient, respectively. The vertical displacement of rail under 90 °C/m reaches 0.72 mm, which is about six times larger than that under −45 °C/m.

(2) Because of the geometric constraint of limiting structures, the maximum bending stresses of the slab occur near the end of the slab under a positive temperature gradient, but that occurs in the middle of the slab under a negative temperature gradient. The maximum bending stress of the slab is 1.37 MPa, which is about 48% of the allowable concrete tension stress of 2.85 MPa of C60 grade concrete. Therefore, the slab stress is critical for the slab track design and should be considered.

(3) The periodic deformation of the slab induces periodic changes in the interlayer stiffness and contact status. With the change of interlayer contact status, the stiffnesses under rail and slab transit into periodic distribution like the deformation of the slab.

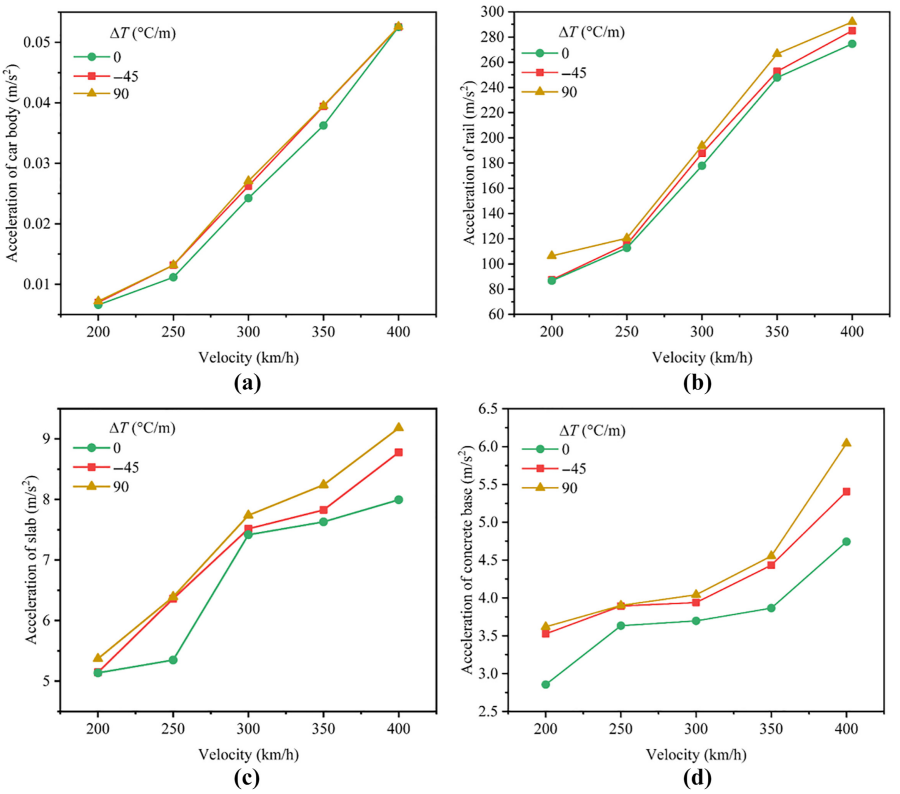

Note(s): (a) Acceleration of car body; (b) acceleration of rail; (c) acceleration of slab; (d) acceleration of concrete base

Source(s): Authors' own work

Figure 10.
The relation between the maximum vertical acceleration and train velocity for typical temperature loads, i.e. $\Delta T = -45, 0, 90$ ℃/m

(4) The maximum dynamic responses significantly increase with the rise in train velocities of the slab track. However, compared with the constant temperature, the maximum dynamic responses under the temperature gradient only increase slightly. The maximum wheel-rail vertical force, the rate of wheel load reduction and the derailment coefficient satisfy the requirements of each response index.

The main practical significance of this work for engineering applications is that the initial irregularity can be rationally preset according to the deformation curves presented in this paper during fine adjustment. Additionally, the measured data can be corrected to partially offset the periodic irregularity during the operational stage.

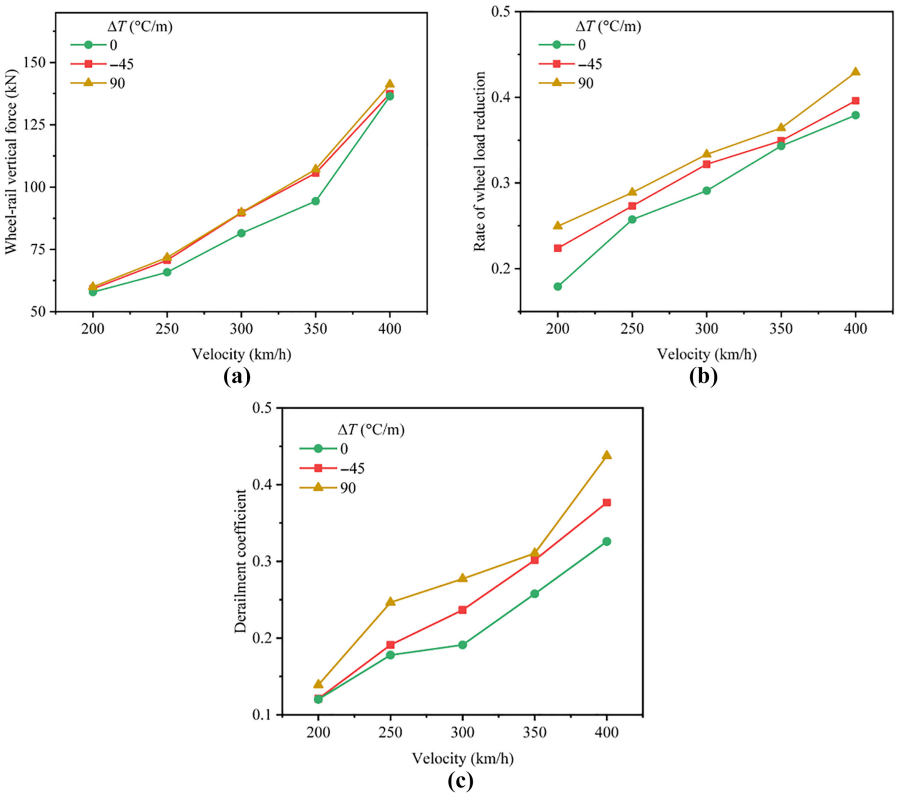

Figure 11.
The relation between maximum dynamic responses of running safety and train velocity for typical temperature loads, i.e. $\Delta T = -45, 0, 90$ °C/m

Note(s): (a) Wheel-rail vertical force; (b) rate of wheel load reduction; (c) derailment coefficient

Source(s): Authors' own work

References

GB 50010-2010 (2010). *Code for design of concrete structures*. China Architecture & Building Press.

Lei, X., & Noda, N. -A. (2002). Analyses of dynamic response of vehicle and track coupling system with random irregularity of track vertical profile. *Journal of Sound and Vibration*, *258*(1), 147–165. doi: 10.1006/jsvi.2002.5107.

Li, Y., Chen, J., Wang, J., Shi, X., & Chen, L. (2020). Study on the interface damage of CRTS II slab track under temperature load. *Structures*, *26*, 224–236. doi: 10.1016/j.istruc.2020.04.014.

Liu, S., Chen, X., Yang, J., Cai, D., & Yang, G. (2020). Numerical study and in-situ measurement of temperature features of asphalt supporting layer in slab track system. *Construction and Building Materials*, *233*, 117343. doi: 10.1016/j.conbuildmat.2019.117343.

Liu, J., Song, L., Liu, H., Zhang, Q., & Yu, Z. (2023). Long-term temperature acceleration effect of solar radiation heating on chloride transport in the CRTS III multilayer structure.

Construction and Building Materials, *375*, 130956. doi: 10.1016/j.conbuildmat.2023.130956.

Ren, J., Deng, S., Zhang, K., Du, W., & Wu, Q. (2021). Design theories and maintenance technologies of slab tracks for high-speed railways in China: A review. *Transportation Safety and Environment*, *3*(4), tdab024. doi: 10.1093/tse/tdab024.

Ren, J., Li, X., Yang, R., Wang, P., & Xie, P. (2016). Criteria for repairing damages of CA mortar for prefabricated framework-type slab track. *Construction and Building Materials*, *110*, 300–311. doi: 10.1016/j.conbuildmat.2016.02.036.

Song, X., Zhao, C., & Zhu, X. (2014). Temperature-induced deformation of CRTS II slab track and its effect on track dynamical properties. *Science China Technological Sciences*, *57*(10), 1917–1924. doi: 10.1007/s11431-014-5634-x.

TB 10015-2012. (2013). *Code for design of railway continuous welded rail*. Beijing: China Railway Publishing House.

TB 10082-2017 (2017). *Code for design of railway track*. China Railway Publishing House.

TB 10621-2014 (2014). *Code for design of high-speed railway*. China Railway Publishing House.

TB/T 3352-2014 (2014). *PSD of ballastless track irregularities of high-speed railway*. China Railway Publishing House.

Xu, Q. Y., & Li, B. (2012). Study on spatial mechanical characteristic of high-speed railway ballastless slab track on subgrade. *Advanced Materials Research*, *503*, 1010–1015. doi: 10.4028/www.scientific.net/amr.503-504.1010.

Xu, Q., Sun, S., Xu, Y., Hu, C., Chen, W., & Xu, L. (2022). Influence of temperature gradient of slab track on the dynamic responses of the train-CRTS III slab track on subgrade nonlinear coupled system. *Scientific Reports*, *12*(1), 14638. doi: 10.1038/s41598-022-18898-y.

Ye, W., Ren, J., Zhang, P., Zhang, Q., & Li, L. (2022). Review of integrated full life cycle data management and application of the slab tracks. *Intelligent Transportation Infrastructure*, *1*, liac018. doi: 10.1093/iti/liac018.

Yu, Z., Xie, Y., & Tian, X. (2019). Research on mechanical performance of CRTS III plate-type ballastless track structure under temperature load based on probability statistics. *Advances in Civil Engineering*, *2019*, 1–16. doi: 10.1155/2019/2975274.

Zhai, W., & Cai, Z. (1997). Dynamic interaction between a lumped mass vehicle and a discretely supported continuous rail track. *Computers and Structures*, *63*(5), 987–997. doi: 10.1016/s0045-7949(96)00401-4.

Zhang, Y., Wu, K., Gao, L., Yan, S., & Cai, X. (2019). Study on the interlayer debonding and its effects on the mechanical properties of CRTS II slab track based on viscoelastic theory. *Construction and Building Materials*, *224*, 387–407. doi: 10.1016/j.conbuildmat.2019.07.089.

Zhao, L. (2015). Spatial refinement analysis method of high speed railway ballastless track and its application, Doctoral Dissertation. Beijing Jiaotong University.

Zhao, L., Yang, G., Liu, W., & Shi, C. (2024). Analysis of the sensitive factors of periodic deformation of unit ballastless track. *Journal of Railway Engineering Society*, *41*(1), 26–38.

Zhong, Y., Gao, L., & Zhang, Y. (2018). Effect of daily changing temperature on the curling behavior and interface stress of slab track in construction stage. *Construction and Building Materials*, *185*, 638–647. doi: 10.1016/j.conbuildmat.2018.06.224.

Zhu, S., & Cai, C. (2014). Interface damage and its effect on vibrations of slab track under temperature and vehicle dynamic loads. *International Journal of Non-linear Mechanics*, *58*, 222–232. doi: 10.1016/j.ijnonlinmec.2013.10.004.

Zhu, S., Wang, M., Zhai, W., Cai, C., Zhao, C., Zeng, D., & Zhang, J. (2018). Mechanical property and damage evolution of concrete interface of ballastless track in high-speed railway: Experiment and simulation. *Construction and Building Materials*, *187*, 460–473. doi: 10.1016/j.conbuildmat.2018.07.163.

Corresponding author
Zhang Huanxin can be contacted at: zhxthu@163.com